

**A Defective Thesis: Studying the Behaviour of Defects in
Liquid-Crystalline Materials**

by

A. A. S. Green

B.Sc., University of Calgary 2011

M.S., University of Colorado at Boulder 2015

A thesis submitted to the
Faculty of the Graduate School of the
University of Colorado in partial fulfillment
of the requirements for the degree of
Doctor of Philosophy
Department of Physics
2019

This thesis entitled:
A Defective Thesis: Studying the Behaviour of Defects in Liquid-Crystalline Materials
written by A. A. S. Green
has been approved for the Department of Physics

Prof. Noel Clark

Who knows

Please, someone

Date _____

The final copy of this thesis has been examined by the signatories, and we find that both the content and the form meet acceptable presentation standards of scholarly work in the above mentioned discipline.

Green, A. A. S. (Ph.D., Physics)

A Defective Thesis: Studying the Behaviour of Defects in Liquid-Crystalline Materials

Thesis directed by Prof. Noel Clark

Often the abstract will be long enough to require more than one page, in which case the macro “\OnePageChapter” should *not* be used.

But this one isn’t, so it should.

Dedication

To all of the fluffy kitties.

Acknowledgements

Here's where you acknowledge folks who helped. But keep it short, i.e., no more than one page, as required by the Grad School Specifications.

Contents

Chapter

1	Introduction	1
2	Bent-Core Characterization	2
2.1	Introduction and Context	2
2.1.1	Characterization	2
2.1.2	Modelling	3
2.1.3	Optical Texture Analysis	3
2.1.4	Polarization Reversal Current	5
2.1.5	X-Ray Scattering	6
2.1.6	Resonant Soft X-ray Scattering	7
2.1.7	Comparison to Previous Phases	9
2.1.8	Remaining Mysteries and Inconsistencies	9
2.2	Homologous Series of PAL30	9

Appendix

Tables

Table

Figures

Figure

- 2.1 Three distinctive optical textures of PAL30 at zero field (b,e,h) and with a field applied into (a,d,g) and out of (c,f,i) of the plane of the cell. *still have to fix up this figure* 3
- 2.2 Optical tilt of PAL30 vs. applied field. The Sm1 phase shows no electrooptic response in weak fields $E < E_{\text{th}}$. Fields $E > E_{\text{th}}$ induce an electroclinic tilt and result in the formation of chiral domains. E_{th} , which becomes smaller with decreasing T (inset), matches closely E_{sat} , the field at which the induced polarization saturates, extracted from Figure ??(d). The Sm2 phase exhibits a chiral electroclinic effect near $E = 0$ and hysteresis in the field-induced helix unwinding to the $\text{SmC}_\text{S}P_\text{F}$ state. 10

2.3	Polarization-reversal current of PAL30. A 40 Hz triangular voltage with an amplitude of 72 V was applied to PAL30 in a 4.5 μm Instec cell. The voltage zero-crossing is at $t = 0$. Three (ferrielectric) current peaks are visible from approximately 110 °C to 99 °C, two (antiferroelectric) peaks from 99 °C to 83 °C, and a single (ferroelectric) peak from 83 °C to 60 °C. The corresponding liquid crystal phases are indicated schematically using the same color scheme as in Figure 1. Three polarization switching peaks are understood to be associated with helical unwinding (see the discussion of the SmC _{FI1} [*] calamitic phase in Takazoe et al. [?]), in contrast with the SmC _{α} [*] calamitic phase, which displays antiferroelectric (two peak) behaviour [?]. Though we believe the Sm2 is best described as an incommensurate Sm(CP) _{α} phase, the pitch (\approx 2.8-layer) is much closer to the 3-layer pitch of the SmC _{FI1} [*] than the Sm _{α} [*] calamitic phases (typically 5–50 layers), which may explain why we see ferrielectricity.	11
2.4	test	12
2.5	X-ray scattering from PAL30. (a) SAXS gives a peak from the smectic layer ordering at $q = q_0$. The RSoXS peak at q_H indicates that there is superlayer orientational ordering with periodicity d_H in the Sm2 phase. In general, superlayer orientational modulation in a smectic generates RSoXS peaks at wavevectors along the layer normal at $q(l, m) = l(2\pi/d_0) \pm m(2\pi/d_H)$ [?]. The observation of an RSoXS reflection at $q = q(0, 1)$ and the absence of an Umklapp peak at $q = q(1, -1)$ in the Sm2 confirms a superlayer helix with a scattering amplitude modulation due to the smectic layering that is undetectably weak. (b) Temperature dependence of resonant scattering. The helix peak at $q_H \approx 1/(2.8d_0)$ becomes diffuse in the Sm3 phase. Splitting of the bilayer peak at q_B , which would indicate helical precession of the bilayer structure, is not observed.	13

- 2.6 Resonant soft X-ray scattering (RSoXS) of PAL30 observed in the Sm1 phase ($T = 113^\circ\text{C}$). This image is characterisitic of the phase. The absence of any resonant scattering features is characteristic of the Sm1 showing that there are no periodic structures present. 14
- 2.7 Diffractogram from PAL30 cooling run carried out at the Berekely facilities in the co-existance region between Sm1 and Sm2. Periodic features are seen at $q \approx 0.004 \text{ \AA}^{-1}$ and $q \approx 0.006 \text{ \AA}^{-1}$ 15
- 2.8 The peaks seen at 102°C in Figure 2.7 disappear as the beam-line energy is scanned through a range of values, confirming that they are resonant, i.e./ they correspond to periodicities in *orientation* not *density*. 16
- 2.9 Resonant soft X-ray scattering (RSoXS) of PAL30 observed vs. temperature on cooling. The plot was generated from a temperature series of 2D diffractograms that were azimuthally averaged, then interpolated and plotted in q -space with corresponding real-space coordinates ($d = 2\pi/q$). Above 110°C , we observe no scattering features, indicating the absence of resonant structures periodic in this d -range. On cooling below 110°C , a scattering arc appears at $d = 148 \text{ \AA}$, corresponding to about three smectic layer spacings. This reflection persists on further cooling but becomes weaker and disappears at 99°C . At 105°C , a second feature appears (at $d = 107 \text{ \AA}$) corresponding to two smectic layer spacings. This feature shifts to smaller q , and then disappears at the transition to the crystal phase at 65°C . In the q range we investigated (corresponding to 50 \AA to 1256 \AA), we see no other orientational modulations. 17

2.10 X-ray scattering from PAL30. (a) SAXS gives a peak from the smectic layer ordering at $q = q_0$. The RSoXS peak at q_H indicates that there is superlayer orientational ordering with periodicity d_H in the Sm2 phase. In general, superlayer orientational modulation in a smectic generates RSoXS peaks at wavevectors along the layer normal at $q(l, m) = l(2\pi/d_0) \pm m(2\pi/d_H)$ [?]. The observation of an RSoXS reflection at $q = q(0, 1)$ and the absence of an Umklapp peak at $q = q(1, -1)$ in the Sm2 confirms a superlayer helix with a scattering amplitude modulation due to the smectic layering that is undetectably weak. (b) Temperature dependence of resonant scattering. The helix peak at $q_H \approx 1/(2.8d_0)$ becomes diffuse in the Sm3 phase. Splitting of the bilayer peak at q_B , which would indicate helical precession of the bilayer structure, is not observed.

Chapter 1

Introduction

Chapter 2

Bent-Core Characterization

To Do: - [] additional work on homologous series (do the birefringence/PRC of PAL29 next week, so we can include it/get Noel thinking about it. - [] Write list of remaining mysteries (wait until we can get out book) - [] outline characterization section (can't do too much without my harddrive, but we can look at the paper and supplement and decide where to put the figures.) Saturday, Dec 29 2018 - [] Read MCLC papers again and memo them for inclusion. - [] Find articles discussing chirality from a mathy and non-mathy perspective, Saturday, Dec 29 2018 - []

2.1 Introduction and Context

- Find original synthesis paper - Talk to Carsten about why they synthesized this phase, so we can include the motivation. - Chirality? (I need to think carefully about chirality, and spontaneous chirality, as this forms a lot of the interesting things about this phase.) - Time for the knives to come out. Discuss their original PRL paper and subsequent MCLC, point out all the reasons for their shitty characterization. We can really go into depth here.

2.1.1 Characterization

-brief summary of characterization before I joined. (Need to decide how in depth we want to do this i.e. narrative focus, or concise. I'm leaning towards concise actually. This isn't a history lesson, it is a textbook entry on PAL30. -look at Mike's NTB characterization chapter for inspiration here.

2.1.2 Modelling

-talk to Matt about this, how does Spartan work? -can he recommend a reference that shows how calculating the smectic layer spacing from this way was actually useful?

2.1.3 Optical Texture Analysis

The optical textures of planar-aligned (bookshelf) cells of PAL30 were studied using PLM. Upon cooling from the isotropic, the Sm1 phase grows in (at 175 °C) as bâtonnets, giving a smooth, focal-conic texture typical of an orthogonal fluid smectic (Figure ??(f)). However, given the large value of the estimated molecular tilt, θ_{xray} , the Sm1 is probably a de Vries smectic. In planar-aligned cells, there is no observable field-induced change of the in-plane birefringence, $\Delta n = n_{\parallel} - n_{\perp}$, in small applied electric fields (Figure ??(f)), or in the optic axis orientation, θ_{opt} (Figure 2.2).

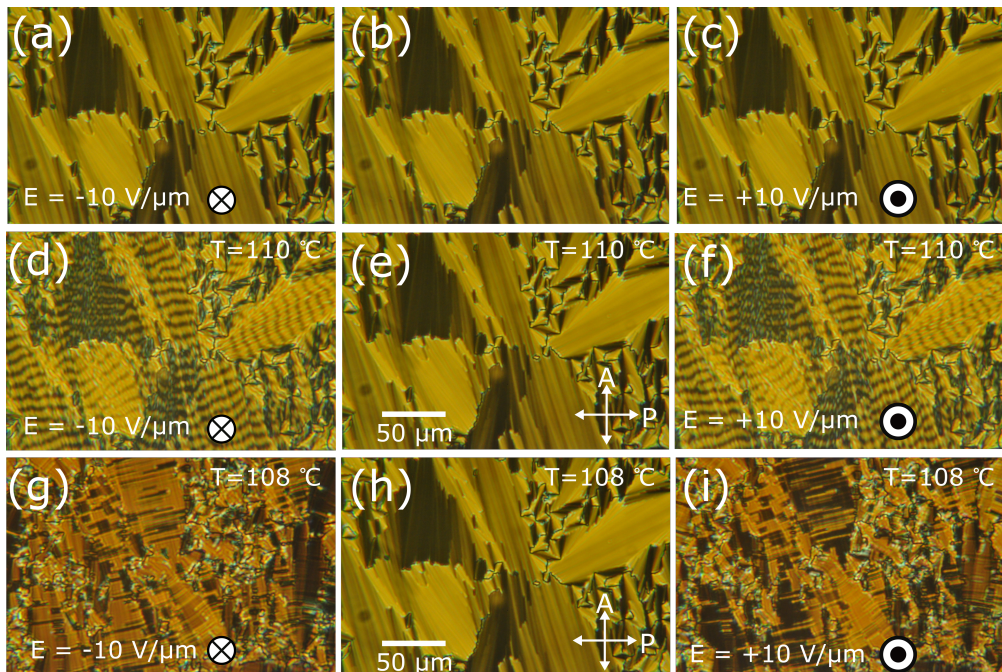


Figure 2.1: Three distinctive optical textures of PAL30 at zero field (b,e,h) and with a field applied into (a,d,g) and out of (c,f,i) of the plane of the cell. **still have to fix up this figure**

Below 115 °C, a threshold field, E_{th} , above which a first-order structural change marked by the appearance of chiral conglomerate domains occurs, becomes experimentally accessible. These

domains are polar and exhibit a uniform, saturated optic axis tilt on the order of $\theta_{\text{opt}} \approx 18^\circ$ from the layer normal, implying that the achiral, untilted Sm1 phase transforms in the field to a B2-like, homochiral $\text{SmC}_S P_F$ state (Figure S1(c)) [?]. The field-induced left- and right-handed domains form a “tiger stripe” pattern (Figures ??(e,g)). The local domain handedness in this unusual conglomerate texture is apparently locked in after the first few field cycles. This bias is due to a chiral memory effect at the surface since, as Figures ??(d) and 2.2 show, the sub-threshold bulk state has an achiral field response, with a linear polarization current (implying $P \propto E$) and no detectable reorientation of the optical tilt. E_{th} decreases strongly on cooling as the transition to the Sm2 phase is approached, as shown in the inset of Figure 2.2.

In the lower part of the Sm1, and throughout the Sm2, Sm3 and Sm4 phases, the birefringence increases on application of an electric field, as seen in Figure ??(c), changing from yellow to orange. Measurements of Δn at $E = 0$ and $E = 20 \text{ V}/\mu\text{m}$ (Figures ??(c) and S6), show that the birefringences in the lower temperature phases with and without an applied field are of the order of $\Delta n_{\text{on}} \sim 0.12$ and $\Delta n_{\text{off}} \sim 0.10$. Assuming that the field-on $\text{SmC}_S P_F$ state (Figures ??(n–p) and S1) gives a uniform director orientation with the optic axis in the plane of the cell, then $\Delta n \sim 0.12$ would correspond to the maximal birefringence $n_3 - n_1$ of the $\text{SmC}_S P_F$ state. Modeling the bent-core molecule as two uniaxial, birefringent rods connected with an opening angle of Ψ , and tilting this molecule from z by an angle θ , we have calculated the birefringence of all of the states shown in Figure ?. If the Sm1 phase is assumed to be a de Vries SmA, with azimuthally averaged molecules distributed on a tilt cone of angle θ , the best fit to the measured birefringence values Δn_{on} and Δn_{off} is obtained with $\Psi = 150^\circ$ and $\theta = 15^\circ$. The calculated birefringence as a function of temperature is shown in Figure S6.

The transitions between the smectic phases are difficult to see when $E = 0$ because they are all orthogonal in appearance, with an optic axis along z , and have similar birefringence. At the transition from Sm1 to the Sm2 phase, however, arbitrarily small electric fields induce molecular tilt in the (Figure 2.2), leading to the formation of optically distinct, conglomerate chiral domains with opposite tilt (Figures ??(h–j)), again corresponding to a field-induced transition to a $\text{SmC}_S P_F$

state. The birefringence and orthogonal appearance of the Sm2 ground state are consistent with the helical superlayer structure indicated by RSoXS.

The texture and birefringence of the Sm3 phase in the absence of field are consistent with the $\text{SmC}_\text{A}P_\text{A}$ bilayer structure indicated by RSoXS. The field-induced conglomerate domain morphology in both the Sm2 and Sm3 phases is distinct from that of the undulating Sm1 tiger stripes, with straight domain boundaries that tend to form parallel to the layers, as in an antiferroelectric calamitic being driven to a ferroelectric state [?]. The optical tilt in these domains is found to be $\theta_{\text{opt}} \sim 18^\circ$.

The response to applied field changes dramatically again at the transition from Sm3 to Sm4, with no visible brush rotation or evidence of domain formation at any E . The birefringence in the Sm4 phase increases continuously with field, saturating at a value comparable to that observed in the field-induced Sm2 and Sm3 conglomerate domains.

PAL30 transitions into a SmA-like phase from the isotropic phase at 174 °C. This phase is optically confirmed to be smectic as the smectic layer undulations give rise to characteristic stripes parallel to the layer normal. These smectic domains grow in as batonnets fix accent, which is again, characteristic to SmA phases. Further cooling results in the development of “tiger stripe” textures on application of high fields (fields larger than some temperature dependent threshold voltage).

These “tiger stripe” textures are unique to the PAL30 molecule, and are characterized by wavy undulations of alternating bright and dark regions that form parallel to the smectic layers. Though the specific dynamics that set the size of these tiger stripes is currently unknown, they are thought to form during a transition to chirality, that will be discussed in more detail.

2.1.4 Polarization Reversal Current

The polarization reversal current, measured with a triangular applied field, is shown vs. temperature in Figures ??(d) and S7. Upon cooling from the isotropic, a single current bump centered about $E = 0$ first appears at lower temperatures in the Sm1 phase, indicating a Langevin-type field-induced orientation of \mathbf{P} , with a linear response near $E = 0$ and the current vanishing

when \mathbf{P} becomes saturated (for $E \geq E_{\text{sat}}$). Significantly, E_{sat} is similar in magnitude to E_{th} , the threshold field required for the Sm1 transition to chirality observed optically (Figure 2.2, inset), indicating that the field first orders the Langevin system of initially azimuthally random molecular polarizations, with the Sm1 remaining in an achiral state, and that the phase becomes chiral only at higher fields, once \mathbf{P} is saturated (Figure S8). Upon entering the Sm2, this polarization bump splits into three peaks roughly centered about $E = 0$, coalescing into two peaks on cooling through the Sm3. PAL30 thus transforms on cooling from the non-polar Langevin ground state of the Sm1, where $P = 0$ is enforced by entropy, to energetically stabilized ground states in which the spatial average of $\mathbf{P}(\mathbf{r})$ in the absence of applied field is also zero: the incommensurate helical winding of the polarization in the Sm2, and the antiferroelectric bilayer structure in the Sm3. At the transition to the Sm4, a single, broad current peak reappears, characteristic of the block polarization switching of a ferroelectric ground state that is surface-stabilized with \mathbf{P} parallel to the cell plates at $E = 0$, such as occurs in the orthorhombic SmAP_F phase [?]. The absence of brush rotation during the field-induced reorientation of the polarization in Sm4 is consistent with achiral SmC_AP_F superlayer organization.

2.1.5 X-Ray Scattering

– another figure highlighting the tiger stripes Undoubtedly, the most powerful probe in revealing the nanoscale structure of these phases of matter is light, specifically, light small enough to resolve this nanoscale structure: X-rays. (digression on Rayleigh resolution/scattering theory?)

For the characterization of PAL30, we used both Small Angle X-ray Scattering (SAXS) and Resonant Soft X-ray Scattering (RSoXS). For the SAXS, we used the Synchtron Source at ZZ, confirming these diffractograms with a ZZ (in house) source, shown in Figure XX.

include multifig with all the traces on it

As SAXS reveals the underlying electron density structure, it is a powerful, though oftentimes, blunt tool for revealing the phase structure. For PAL30, we observed only a single Bragg peak at $\approx 50 \text{ \AA}$. The absence of harmonic peaks indicate that the underlying electron density is very close

to being perfectly sinusoidal, allowing for decomposition into a singular Fourier wavelength which corresponds to the smectic layer spacing.

- include all the SAXS figures, (can we replot them onto the same graph?) - Discuss smectic layer spacing, talk about what else we can determine from this
- include RSOXS figures (main one).
- orientational at approx $2.8d_0$, talk about what this could be? Chew the fat on this one.

2.1.6 Resonant Soft X-ray Scattering

Resonant soft X-ray scattering (RSoXS), as discussed in Section ??, is sensitive to periodicities in the orientation of the underlying molecules. The RSoXS scans for PAL30 were carried out by Dr. Michael Tuchband at the Synchrotron Source in Berkeley. **include relevant preamble from the supplement about the Berkeley facilities** X-ray scattering from PAL30 is shown in Figures ??(b) and S3. Upon cooling from the isotropic, a single, non-resonant SAXS peak appears at 175°C , at a wavevector q_0 corresponding to Bragg scattering from the smectic layers in the Sm1 phase with spacing $d_0 = 2\pi/q_0 = 48\text{\AA}$. The layer spacing increases slightly on cooling to the crystal phase at 65°C and is consistently smaller than the calculated molecular length, $l = 59.9\text{\AA}$, throughout this temperature range, suggesting that the molecules are tilted in all of the smectic phases, to first order by an average amount estimated using $\theta_{\text{xray}} = \cos(d_0/l)$ of 33° (see Figure S4). In the Sm1 temperature range ($110^\circ\text{C} \leq T \leq 175^\circ\text{C}$), there are no RSoXS scattering features that would indicate a superlayer periodic structure (see Figure S2 and the Supplemental video).

At the transition to the Sm2 phase, at 110°C , marked by a distinct enthalpy peak in the DSC (Figure S5), a single, sharp resonant peak appears at $q_H = 0.042\text{\AA}^{-1}$, corresponding to a molecular orientational structure with a period $d_H = 148\text{\AA} \approx 2.8d_0$ that is incommensurate with the smectic layer spacing (Figure 2.5(b)). Below 104°C , this reflection becomes weaker and another sharp, resonant reflection at higher q grows in, the coexistence indicating a first-order transition to the Sm3 phase. This second Bragg peak, which persists down to the crystal phase, has a wavevector $q_B \approx q_0/2$, indicative of a commensurate, bilayer orientational structure in the Sm3 and Sm4 phases. Below 99°C , the incommensurate peak broadens dramatically and moves

to higher q , indicating the presence of short-ranged, Sm2-like helical fluctuations persisting in the Sm3 phase, and disappears at the transition to the Sm4 phase at 83 °C. The Sm4 phase exhibits only the bilayer RSoXS reflection at q_B .

The RSoXS scattering from a single layer can be analyzed, following Levelut and Pansu, in terms of a monoclinic second-rank tensor with a principal axis tilted from and then azimuthally rotated about the layer normal [?, ?, ?]. Scattering from a stack of such layers is calculated by summing over the contributions of the individual layers at different z . Resonant scattering peaks from azimuthally periodic arrangements are found at wavevectors along z , $q(l, m) = l(2\pi/d_0) \pm m(2\pi/p)$, where p is the pitch. In principle, resonant scattering should appear at all values of l (harmonics of q_0), and at values of $m = 0, \pm 1, \pm 2$ that depend on the superlayer structure. In an incommensurate, helical structure, like the SmC α phase, only the fundamental and harmonic peaks at $q(l = 0, m = +1, +2)$ and the Umklapp peaks at $q(l = +1, m = -1, -2)$ are found in the range $0 < q(l, m) < q_0$. If the resonant scatterers are confined to lie precisely on layers spaced by d_0 , then the intensities of these peaks will be identical [?]. Out-of-layer molecular positional fluctuations, and, in particular, those for which there is a coupled azimuthal orientation that keeps the molecule on the helix, $\delta\phi = (2\pi/p)\delta z$, reduce the intensities of the resonant harmonic peak at $2q_H$ and of the Umklapp peaks at $q_0 \pm q_H$, relative to that of the fundamental at q_H [?]. In our RSoXS scans of these peaks, only the fundamental is seen above the background, so that only the upper limit of the intensity ratio of the Umklapp and fundamental peaks can be estimated. From the RSoXS heating scan of Figure 2.5(a), we find $I_U/I_F \lesssim 0.03$, implying a very weak fractional modulation of the density of helical scatterers, ρ , due to fluctuations in the smectic layering $\sqrt{\langle \delta\rho^2 \rangle}/\rho_0 < 0.17$. The absence of the harmonic peaks places a similar limit on how much the density modulation of helical scatterers deviates from being purely sinusoidal.

These features were confirmed to be resonant peaks by scanning the beam-line energy through a range, as shown in Figure 2.8.

discussion of what this all means, with theory digression to explain the flucuations

2.1.7 Comparison to Previous Phases**2.1.8 Remaining Mysteries and Inconsistencies**

-Look at list that I've written down here. (Should work on this firstish, so we can send it to Leo.)

2.2 Homologous Series of PAL30

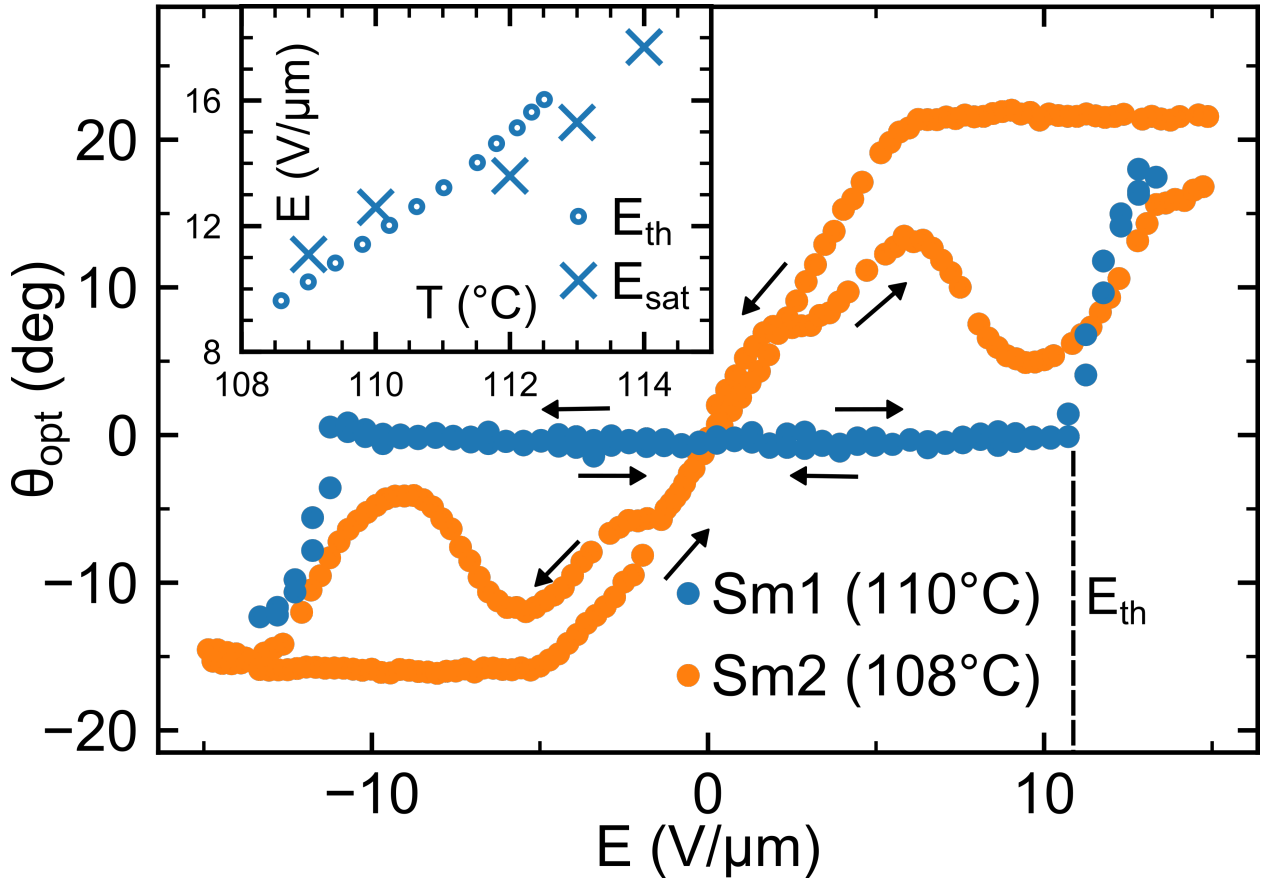


Figure 2.2: Optical tilt of PAL30 vs. applied field. The Sm1 phase shows no electrooptic response in weak fields $E < E_{\text{th}}$. Fields $E > E_{\text{th}}$ induce an electroclinic tilt and result in the formation of chiral domains. E_{th} , which becomes smaller with decreasing T (inset), matches closely E_{sat} , the field at which the induced polarization saturates, extracted from Figure ??(d). The Sm2 phase exhibits a chiral electroclinic effect near $E = 0$ and hysteresis in the field-induced helix unwinding to the $\text{SmCS}P_F$ state.

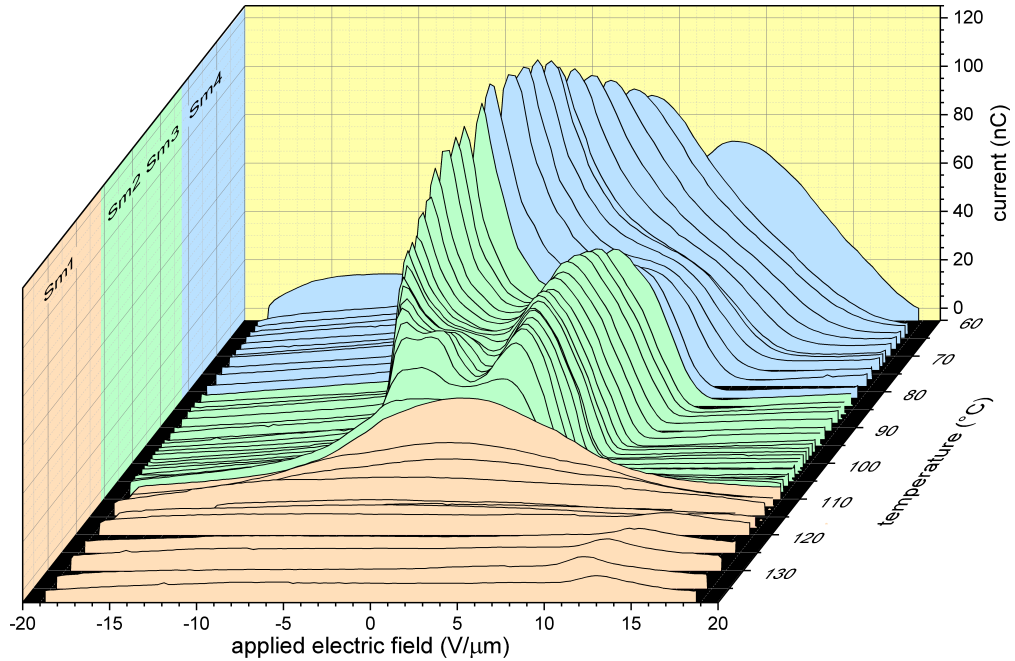


Figure 2.3: Polarization-reversal current of PAL30. A 40 Hz triangular voltage with an amplitude of 72 V was applied to PAL30 in a $4.5 \mu\text{m}$ Instec cell. The voltage zero-crossing is at $t = 0$. Three (ferrielectric) current peaks are visible from approximately 110°C to 99°C , two (antiferroelectric) peaks from 99°C to 83°C , and a single (ferroelectric) peak from 83°C to 60°C . The corresponding liquid crystal phases are indicated schematically using the same color scheme as in Figure 1. Three polarization switching peaks are understood to be associated with helical unwinding (see the discussion of the $\text{SmC}_{\text{FI}1}^*$ calamitic phase in Takazoe et al. [?]), in contrast with the SmC_α^* calamitic phase, which displays antiferroelectric (two peak) behaviour [?]. Though we believe the $\text{Sm}2$ is best described as an incommensurate $\text{Sm}(\text{CP})_\alpha$ phase, the pitch (≈ 2.8 -layer) is much closer to the 3-layer pitch of the $\text{SmC}_{\text{FI}1}^*$ than the Sm_α^* calamitic phases (typically 5–50 layers), which may explain why we see ferrielectricity.

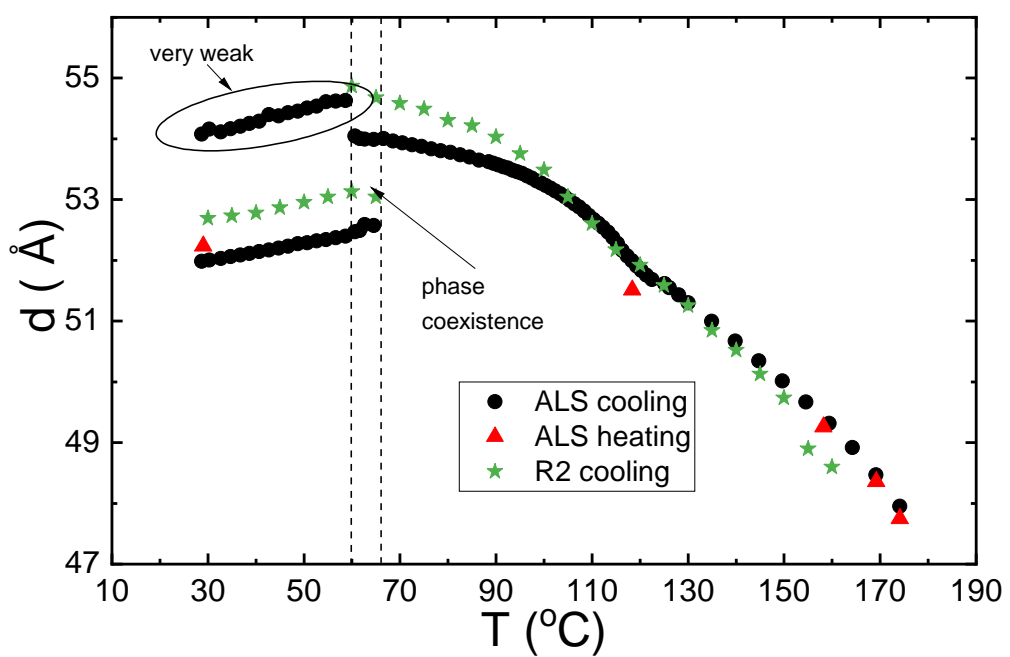


Figure 2.4: test

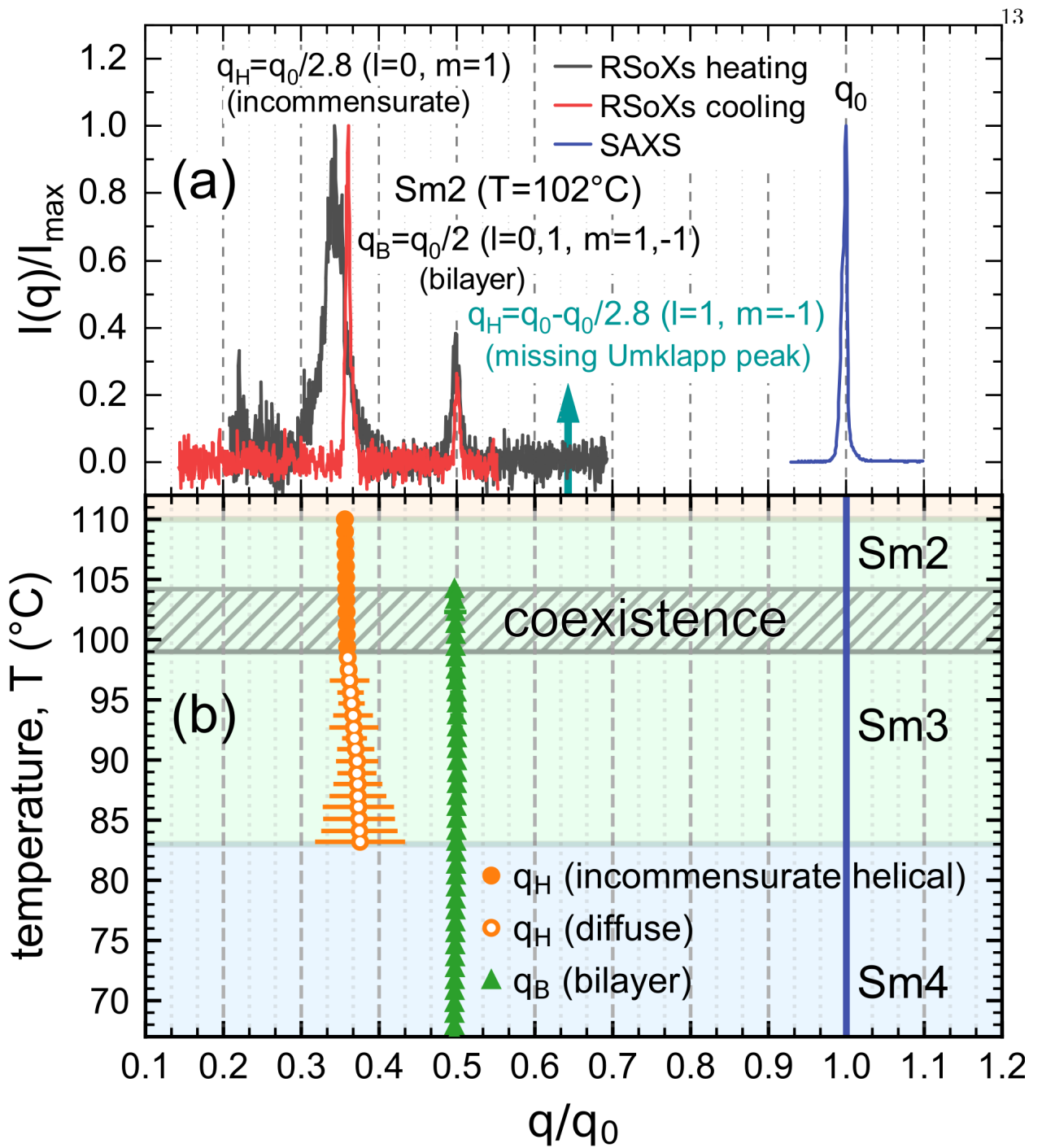


Figure 2.5: X-ray scattering from PAL30. (a) SAXS gives a peak from the smectic layer ordering at $q = q_0$. The RSoXS peak at q_H indicates that there is superlayer orientational ordering with periodicity d_H in the Sm2 phase. In general, superlayer orientational modulation in a smectic generates RSoXS peaks at wavevectors along the layer normal at $q(l, m) = l(2\pi/d_0) \pm m(2\pi/d_H)$ [?]. The observation of an RSoXS reflection at $q = q(0, 1)$ and the absence of an Umklapp peak at $q = q(1, -1)$ in the Sm2 confirms a superlayer helix with a scattering amplitude modulation due to the smectic layering that is undetectably weak. (b) Temperature dependence of resonant scattering. The helix peak at $q_H \approx 1/(2.8d_0)$ becomes diffuse in the Sm3 phase. Splitting of the bilayer peak at q_B , which would indicate helical precession of the bilayer structure, is not observed.

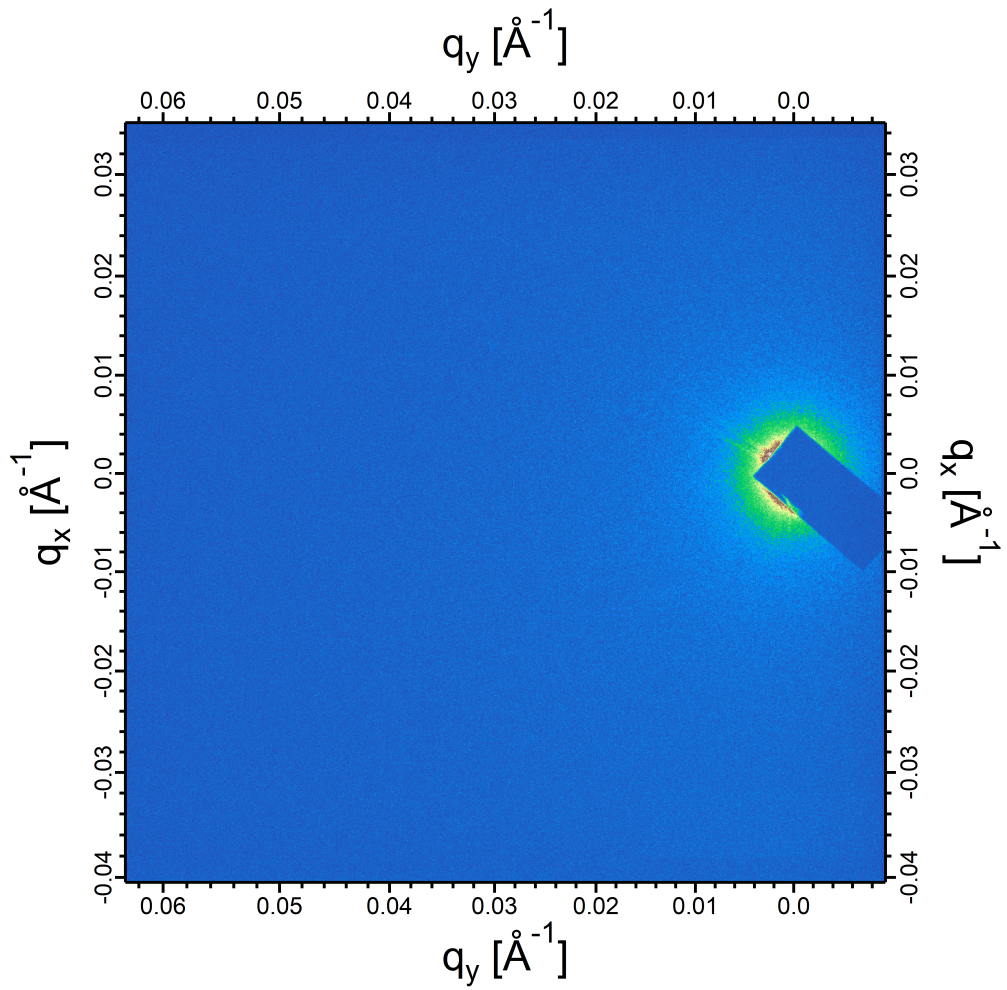


Figure 2.6: Resonant soft X-ray scattering (RSoXS) of PAL30 observed in the Sm1 phase ($T = 113^\circ\text{C}$). This image is characteristic of the phase. The absence of any resonant scattering features is characteristic of the Sm1 showing that there are no periodic structures present.

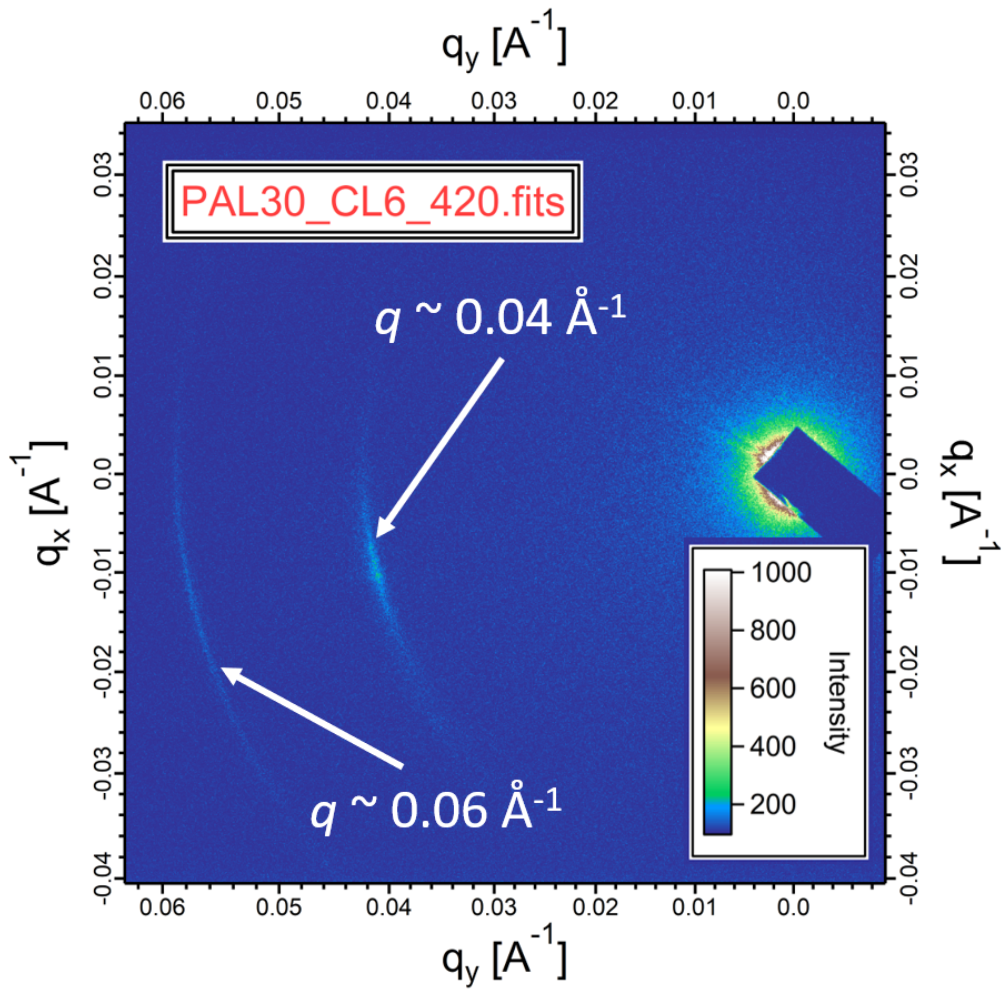


Figure 2.7: Diffractogram from PAL30 cooling run carried out at the Berkeley facilities in the coexistence region between Sm1 and Sm2. Periodic features are seen at $q \approx 0.004 \text{ \AA}^{-1}$ and $q \approx 0.006 \text{ \AA}^{-1}$.

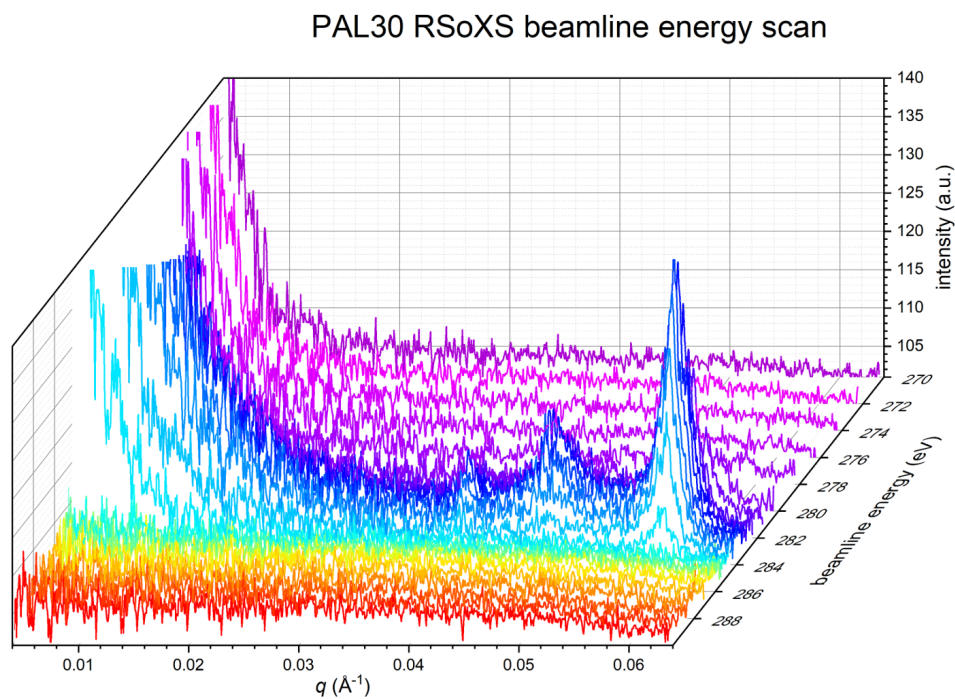


Figure 2.8: The peaks seen at 102 °C in Figure 2.7 disappear as the beam-line energy is scanned through a range of values, confirming that they are resonant, i.e./ they correspond to periodicities in *orientation* not *density*.

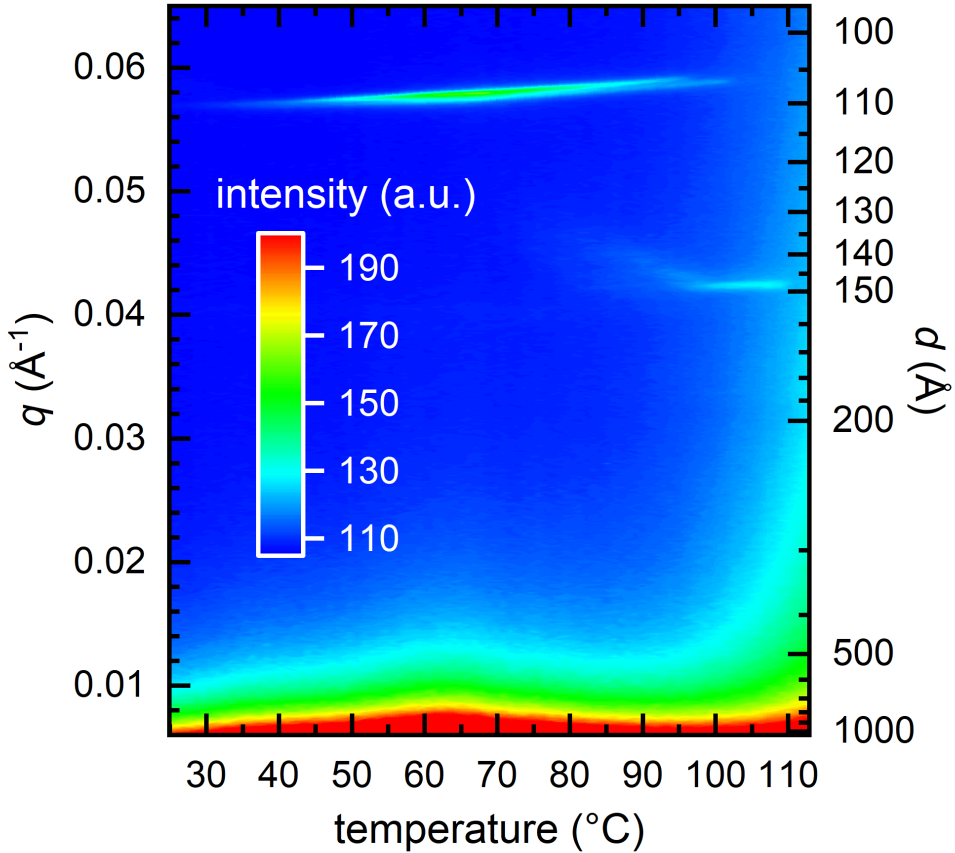


Figure 2.9: Resonant soft X-ray scattering (RSoXS) of PAL30 observed vs. temperature on cooling. The plot was generated from a temperature series of 2D diffractograms that were azimuthally averaged, then interpolated and plotted in q -space with corresponding real-space coordinates ($d = 2\pi/q$). Above 110 °C, we observe no scattering features, indicating the absence of resonant structures periodic in this d -range. On cooling below 110 °C, a scattering arc appears at $d = 148 \text{ \AA}$, corresponding to about three smectic layer spacings. This reflection persists on further cooling but becomes weaker and disappears at 99 °C. At 105 °C, a second feature appears (at $d = 107 \text{ \AA}$) corresponding to two smectic layer spacings. This feature shifts to smaller q , and then disappears at the transition to the crystal phase at 65 °C. In the q range we investigated (corresponding to 50 \AA to 1256 \AA), we see no other orientational modulations.

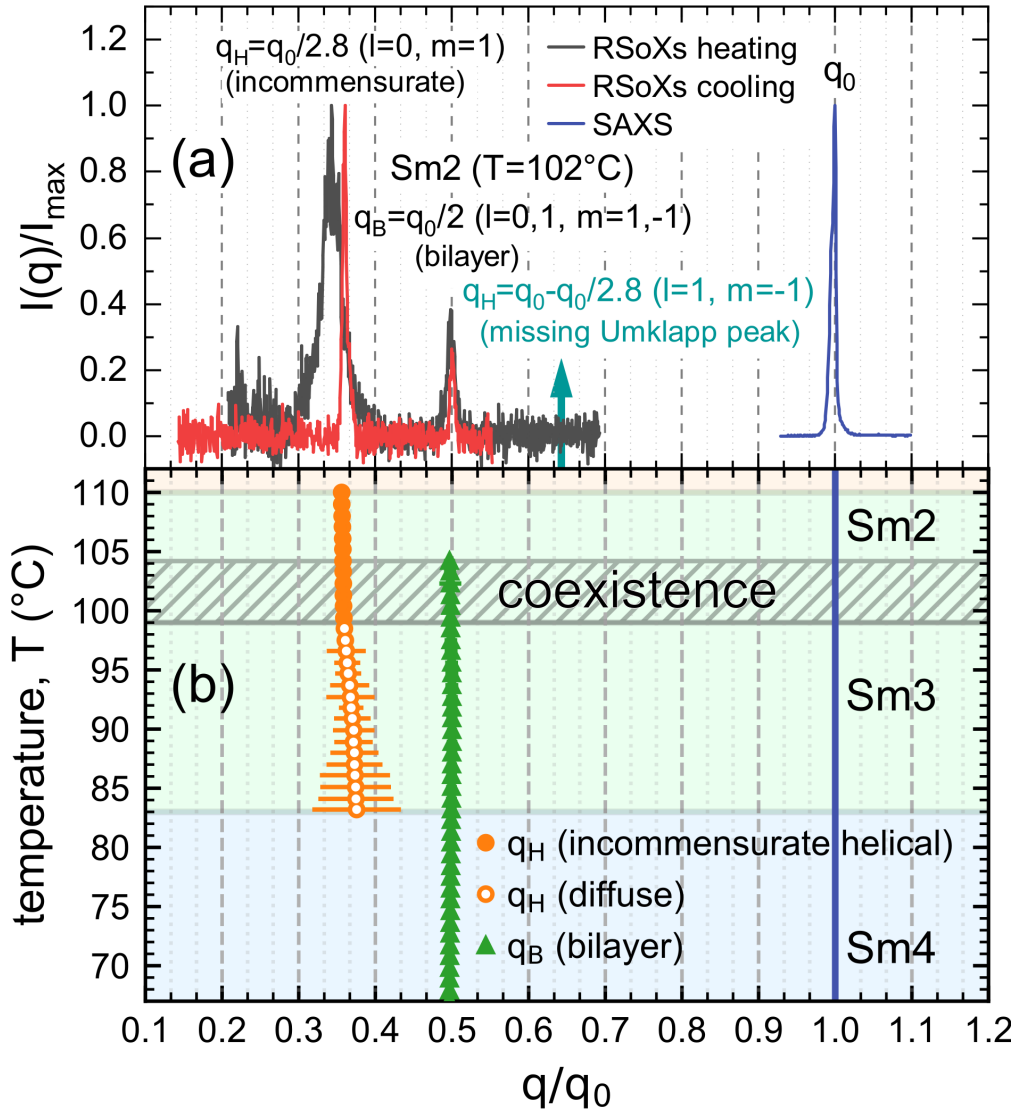


Figure 2.10: X-ray scattering from PAL30. (a) SAXS gives a peak from the smectic layer ordering at $q = q_0$. The RSoXS peak at q_H indicates that there is superlayer orientational ordering with periodicity d_H in the Sm2 phase. In general, superlayer orientational modulation in a smectic generates RSoXS peaks at wavevectors along the layer normal at $q(l, m) = l(2\pi/d_0) \pm m(2\pi/d_H)$ [?]. The observation of an RSoXS reflection at $q = q(0, 1)$ and the absence of an Umklapp peak at $q = q(1, -1)$ in the Sm2 confirms a superlayer helix with a scattering amplitude modulation due to the smectic layering that is undetectably weak. (b) Temperature dependence of resonant scattering. The helix peak at $q_H \approx 1/(2.8d_0)$ becomes diffuse in the Sm3 phase. Splitting of the bilayer peak at q_B , which would indicate helical precession of the bilayer structure, is not observed.